Investigating Mercury's south polar deposits with high-resolution imaging

Evangela E. Shread, Nancy L. Chabot

Johns Hopkins University Applied Physics Laboratory

Introduction

More than two decades ago, Earth-based radar observations of Mercury's polar regions revealed clusters of radar-bright material believed to be water ice [1-3]. The MESSENGER mission provided subsequent data to support the hypothesis that water ice exists in areas of permanent shadow at both poles [4-9]. The Narrow Angle Camera (NAC) of the Mercury Dual Imaging System (MDIS) offers high-resolution imaging of the illumination conditions present at the south pole, which has been lesser studied than the north due to the high eccentricity of MESSENGER's orbit.

Mapping south polar region using NAC data set

A mosaic of the south polar region from 80-90° S was made from 1,090 NAC images acquired during MESSENGER's full orbital mission. The images were combined according to subsolar longitude in order to represent the variations in shadowing over Mercury's solar day. This resulted in fifty mosaics with longitudinal bins of 7° and one with a longitudinal bin of 10°.

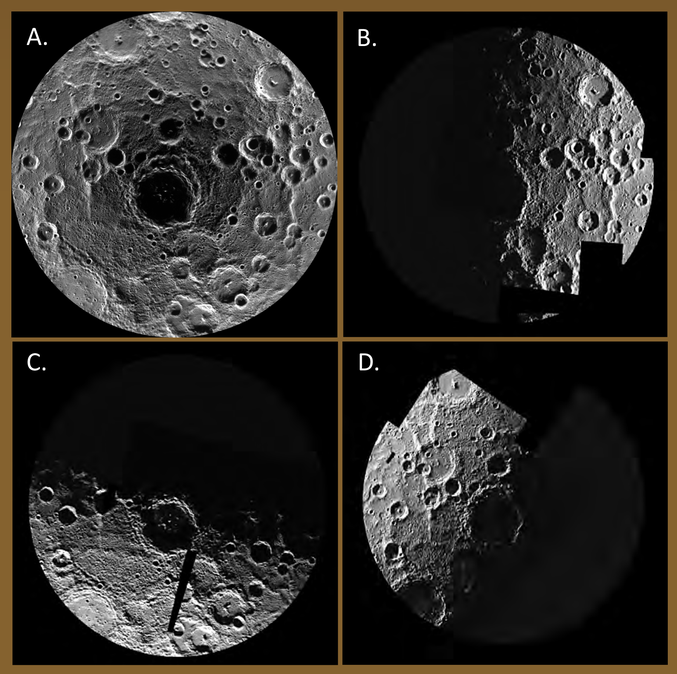

(a) Map of south pole made from NAC images grouped together based on subsolar longitude. Example mosaics correspond to subsolar longitude bins centered at (b) 98° E (c) 203° E, and (d) 322° E.

Illumination conditions

- Each of the 51 mosaics were separated into shadowed and sunlit pixels
- The binary images were weighted according to Mercury's 3:2 spin-orbit resonance
- A correction was applied to account for gaps in coverage
- Mosaics were combined into an average illumination map with a pixel resolution of 200 m

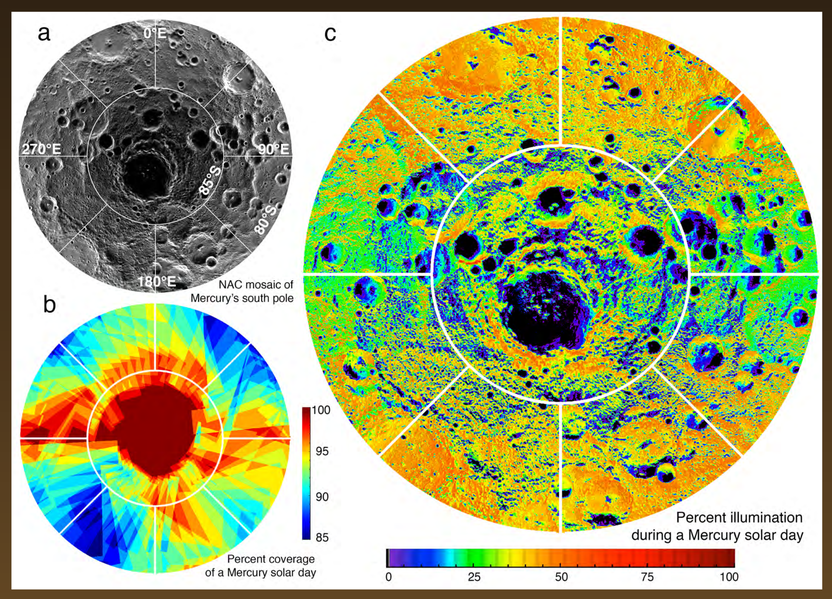

(a) NAC mosaic of Mercury's south pole. (b) Percent coverage in image set over a solar day. (c) Map of percent illumination during one solar day.

Long exposure NAC images

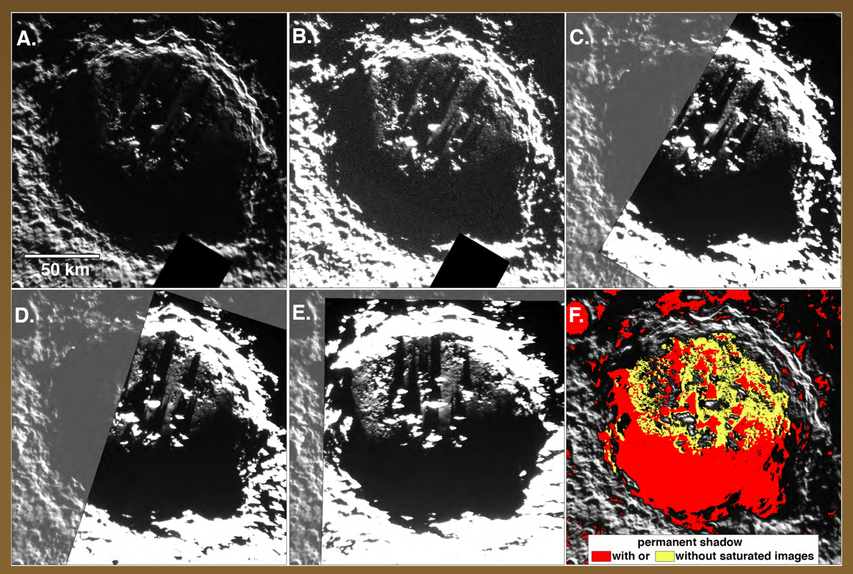

(a) Standard-exposure NAC mosaic of Chao Meng-Fu. (b) Same mosaic, but with brightness and contrast stretch applied. Saturated images taken from 7° longitudinal bins centered on (c) 209.8° E, (d) 197.5° E and (e) 180.3° E. (f) Permanent shadow mapped both with and without saturated images.

- 67 NAC images with exposure times ≥ 250 ms were acquired as part of an effort to image within areas of permanent shadow, focusing mainly on crater Chao Meng-Fu which has a diameter of 180 km
- Saturated images expose dimly lit features between shadows cast by Chao Meng-Fu's central peaks, which are less visible in the standard NAC imaging
- Area of permanent shadow is reduced when saturated images are included

Comparison of radar-bright and permanently shadowed areas

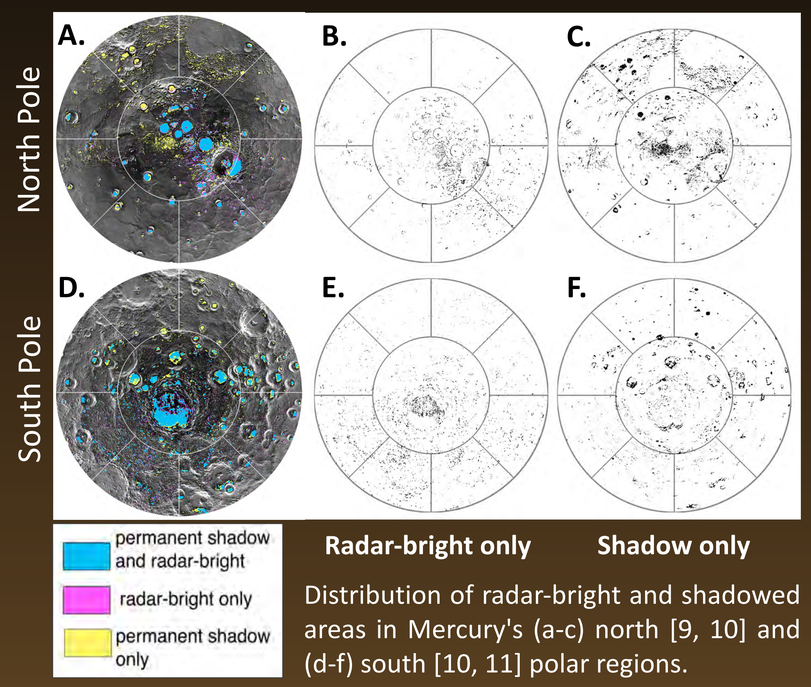

Distribution of radar-bright and shadowed areas in Mercury's (a-c) north [9, 10] and (d-f) south [10, 11] polar regions.

Comparison of radar-bright and shadowed features near Mercury's north and south poles by percentage of region

80-90° latitude	North Pole [9]	South Pole
Radar-bright area	2.2%	4.4% [10,11]
Permanently shadowed area	3.7%	5.7%
Radar-bright deposits in shadow	78.9%	77.3%
Shadowed terrain that is radar-bright	46.4%	45.0%

- The water-ice hypothesis is supported by the observed strong agreement between radar-bright and shadowed areas in the south polar region, which has also been observed in the north polar region. About 77% of radar-bright material is aligned with mapped areas of shadow in the south polar region, and almost 79% align with areas of shadow identified in the north.
- Less than half of the shadowed area in the north and south pole is radar-bright, and the distribution of these areas is uneven in both the north and south polar regions.

Implications

The observed uneven distribution of radar-bright deposits at both the north and south poles could suggest that a recent, large impact event is responsible for the placement of ice on Mercury.

Acknowledgements: NASA DDAP grant NNX15AK89G to N.L.C; APL ASPIRE and NASA/APL intern programs for E.E.S to do this work.

References: [1] Slade, M. A. et al. (1992) *Sci.*, 258, 635-640. [2] Harmon, J. K. and Slade, M. A. (1992) *Sci.*, 258, 640-643. [3] Butler, B. J. et al. (1993) *JGR*, 98, 15,003-15,023. [4] Chabot, N. L. et al. (2012) *GRL*, 39, L09204. [5] Lawrence D. J. et al. (2013) *Sci.*, 339, 292-296. [6] Neumann G. A. et al. (2013) *Sci.*, 339, 296-300. [7] Paige D. A. et al. (2013) *Sci.*, 229. 300-303. [8] Chabot N. L. et al. (2014) *Geology*, 42, 1051-1054. [9] Deutsch et al. (2016) *Icarus*, 280, 158-171. [10] Harmon J. K. et al. (2011) *Icarus*, 211, 37-50. [11] Chabot N. L. et al. (2018) *JGR*, 123, 666-681.